DOI: https://doi.org/10.36722/exc.v1i1.2280

FPGA Implementation of Kalman Filter for Visible Light

Imam Wahyudi[1*], Dwi Astharini[1], Danny M. Gandana[2], Sofian Hamid[1,3], Denny Hermawan[4], Budi Aribowo[5]

[1]Department of Electrical Engineering, University Al-Azhar Indonesia, Jakarta 12110, Indonesia
[2]National Research and Innovation Agency, Indonesia
[3]Institute of High Frequency Technology RWTH Aachen University, Aachen, Germany
[4]Department of Informatics, Faculty of Science and Technology,
University of Al-Azhar Indonesia, Sisingamangaraja, South Jakarta, 12110, Indonesia
[5]Department of Industrial Engineering, Faculty of Science and Technology,
University of Al-Azhar Indonesia, Sisingamangaraja, South Jakarta, 12110, Indonesia
Correspondence Email: wahyudijr1@gmail.com

Abstract

This paper integrates Visible Light (VL) communication with the Kalman Filter (KF) to improve data prediction and estimation accuracy. The implementation utilizes Xilinx FPGA Arty A7 hardware and employs a two-dimensional Linear KF framework. The main objective is to implement VL positioning with a KF algorithm on FPGA using photodetectors (Photodiode and Photoresistor) as measurement sensors. The use of Xilinx FPGA Arty A7 hardware and Xilinx SDK ensures flexibility and reliability in the system. The results demonstrate accurate estimations using Xilinx FPGA Arty A7-35T with the KF algorithm in both 16 LED and 8 LED setups. The performance of the Photodiode LM393 (PD LM393) sensor is comparable to the Photoresistor LM393 (PR LM393). This study optimizes light measurements by combining the sensor-KF algorithm. The evaluation of KF performance, measured by Ro Mean Squared error (RMSE) results, shows that for the 16 LED system, KF with PR LM393 achieves an RMSE of approximately ($\mathbf{1,69\ x\ 10^{-2}\ V}$), indicating accurate estimations. In the 8 LED system, KF with PR LM393 yields an RMSE of around ($\mathbf{1,71\ x\ 10^{-2}}$), ensuring accuracy in estimation. Additionally, the 2D KF approach results in an RMSE of about ($\mathbf{7,8478\ x\ 10^{-1}\ V}$), demonstrating effective noise reduction and precise estimation in the LM393 Photodetector system with 16 LEDs.

Keywords: ***FPGA, Kalman Filter, Positioning, SDK, Verilog, VHDL, Visible Light, Vivado***

1. INTRODUCTION

Wireless communications have undergone a transformative shift by harnessing wireless carriers like Radio Frequency (RF) and Visible Light (VL) waves to transmit data. The escalating demand for high data rates, particularly in indoor environments, has overwhelmed traditional RF systems. In response, innovative strategies such as millimeter waves (mm-wave) and cognitive radios have been adopted to counteract the capacity constraints and spectrum scarcity of conventional RF systems. Furthermore, VL Communication (VLC), which utilizes light sources for both data transmission and illumination, presents itself as a promising alternative.

Notably, VL technology exhibits robust resistance to electromagnetic interference, enjoys unlicensed channels, operates on minimal electrical power, and poses negligible health risks [1], diverse VL Platforms (VLPs) beyond photodetector-dependent ones exist, including those grounded on imaging sensors known as camera sensors. Transmitted VL signals can be received through an image sensor, a matrix, or an integrated circuit of numerous Photodetectors. However, the employment of an imaging sensor necessitates a considerable number of PDs to achieve high-resolution photos, introducing limitations [2], a

key element is the LED, modulating light while being accompanied by a receiver photodetector that adjusts the intensity of optically modulated data. The VLC Channel, constituting the fundamental aspect of the VL Receiver system, facilitates this communication [3], in the transmission process, the modulated signal, acting as a transmitter, is paired with a DC voltage to power the LED. LEDs serve the dual purpose of emitting light and transmitting information. The receiver combines a photodetector and demodulator, wherein the photodetector converts received light into an electrical signal containing messages and noise. While the electrical domain might encapsulate noise comprehensively, a portion of noise stems from the communication channel. This phenomenon arises from the PD's capacity to transform optical noise and signals into electric current [4], integral to this discourse is the FPGA Artix-7/Arty A7 series developed by Xilinx, encompassing versatile Field-Programmable Gate Array (FPGA) devices. A prominent member of the Xilinx 7 Series FPGA family, the Artix-7 offers high performance and flexibility for digital circuit implementation. Reprogrammable FPGA resources enable tailored digital circuit creation catering to specific application requirements. With advanced 28nm architecture, features such as block RAM, Digital Signal Processor (DSP) slices, and configurable Input/Output(I/O) bolster its capabilities [5], facilitating FPGA-based systems' design and implementation is the Vivado Design Suite-HLx Editions, a suite of Xilinx tools supporting intricate system creation [6].

Crucial to wireless communication and FPGA implementation is the application of Hardware Description Languages (HDL). While other HDL have surfaced, Verilog and VHDL (VHSIC (Very High-Speed Integrated Circuit) Hardware Description Language) remain primary standards for documenting, modeling, and logic synthesis of electronic circuits. Their comprehensive use is highlighted by "HDL Chip Design" (1996) by Douglas J. Smith, a pioneering book showcasing examples of both languages for simulation and synthesis [7].

The Photodiode LM393 (PD LM393) Module, integral in robotics, measures brightness and ambient light intensity. PDs offer superior directionality compared to Photoresistors (PR), making PDs adept at locating light sources, while PRs excel at measuring light intensity. The PD module's digital output varies from HIGH to LOW based on ambient light, producing a high level when the light is below a threshold and a low level when it exceeds the threshold [8], on the other hand, the Light Depending Resistor (LDR) LM393 or Photoresistor LM393 (PR LM393) sensor utilizes the LM393 IC as a comparator, which is an electronic component that compares the input voltage with a reference and produces an output based on this comparison. In the LDR LM393 sensor, the output voltage changes based on the resistance of the LDR, which is influenced by the light intensity. By using the comparator, the sensor can generate a digital signal depending on the predetermined threshold. For example, when the light intensity exceeds the set threshold, the sensor output will be high (usually 5V), and when the light intensity is below the threshold, the sensor output will be low (usually 0V) [9], super Bright 5mm LEDs, revered for their exceptional brightness and wide beam angle, find utility in models, illuminations, headlamps, and automotive lighting [10].

Facilitating this fusion of hardware and software is the Xilinx SDK (Software Development Kit). Developed by Xilinx, a key player in programmable hardware, this SDK is tailored for real-time operating system (RTOS) development using Xilinx FPGA hardware. It empowers the creation and customization of BSPs (Board Support Packages) that bridge FPGA hardware and real-time operating systems such as FreeRTOS [11], an indispensable algorithm in this ecosystem is the Kalman Filter (KF), employed to predict future outcomes based on prior data and minimize noise. KF's linear system assumptions, coupled with its capacity to mitigate noise, render it a cornerstone in applications spanning navigation, robotics, and control systems. The integration of KF augments VLC systems by enhancing data accuracy and attenuating noise and fluctuations [12].

UAI's prior work encompassed exploring the application of KF in 3D indoor positioning, while also effectively demonstrating the successful implementation of VL Communication (VLC) Transmitter and Receiver utilizing Xilinx FPGA, this current project represents a fusion of these prior endeavors, integrating VL technology with KF methodology to enhance the precision of data prediction. This integration is anchored in the

Xilinx FPGA Arty A7 hardware platform and employs a sophisticated 2D Linear KF framework. The implementation process encompasses hardware configuration, Photodetectors deployment, programming within the Vivado software, application of the KF algorithm to acquire data, and an extensive simulation of the KF algorithm. The primary objective of this project is to establish a functional VL system using Photodetectors on Xilinx FPGA Arty Hardware, with specific research objectives encompassing efficient data transfer, robust KF program testing, and effective noise reduction in Photodetectors data.

2. METHOD

In this research, the design process involves key stages for implementing the LED light system with the KF algorithm using FPGA. It starts with designing the receiving system and configuring it for FPGA in Vivado. Then, the receiver system for LED design is implemented, generating data. Processed data undergoes analysis. The Arty MicroBlaze block diagram and VHDL Programming are created in Vivado, and KF algorithm integration occurs through Xilinx SDK. This enhances accuracy by reducing noise. Data post-KF implementation is extensively processed, leading to an in-depth analysis of Vivado and SDK results. The conclusion offers insights drawn from the entire iterative journey and After all of the process is finished, the performance of the system can be evaluated.

E. Implementation Process

The process consists of two main steps. Step A involves setting up and implementing the reception system to store data, while Step B focuses on programming and implementing the KF algorithm using data from Step A. Step B is an advanced phase that utilizes the collected data to enhance measurements through the KF algorithm.

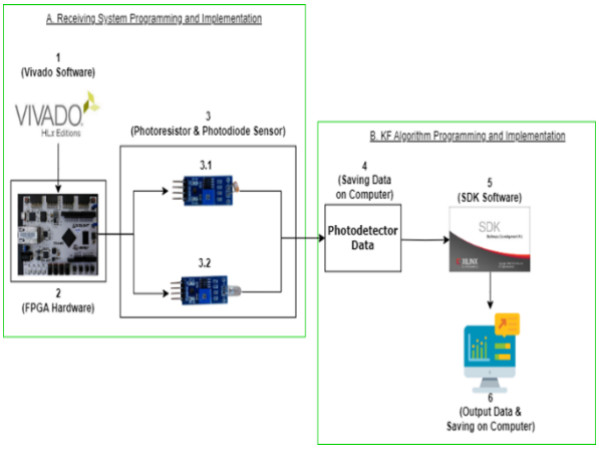

Fig 1. Block Diagram of KF VL Implementation

The Implementation of the Process Contained in Fig 1: (1). Configure Xilinx FPGA Arty A7-35T and Photodetectors, conduct experiments and testing (1-2-3). (2). Read actual data from Photodetectors based on LED light, store and display data on a computer (1-2-3-4). (3). Implement KF System using Xilinx SDK with acquired light reading data (4-5). (4). Collect, process, and present data using the KF system on a computer (6).

Each step outlines specific actions, from configuring hardware to presenting processed data, ensuring a coherent and efficient process.

F. Kalman Filter Algorithm

The KF is an algorithm utilized for predicting or estimating future outcomes through the analysis of previous data. Unlike general filters such as Low Pass Filter (LPF), High Pass Filter (HPF), or Band Pass Filter (BPF), KF operates as an estimator, particularly suited for predicting states within a signal that may contain noise. Within the KF system, a linear framework is assumed. KF's objective is to minimize the mean squared error of estimation for stochastic linear systems, incorporating linear sensor noise. Moreover, it also reduces the squared error function of estimation for linear dynamic systems affected by white measurement and disturbance noise. Its role encompasses the estimation of a dynamic system's state and performance analysis. As detailed in equations, the KF functions as a data processing tool to estimate the state of a dynamic system using measurements that are subject to noise contamination. The filter's primary aim is to enhance the accuracy of estimates by fusing historical information with the latest measurements. Comprising two main segments,

the KF Algorithm consists of the prediction part and the updating part [15], the KF equation utilized in this research is outlined in equations (1) to (6).

Prediction:

$$\hat{x}(k+1|k) = A_t.\hat{x}(k|k) \quad (1)$$

$$P(k+1|k) = A_t.P_t(k|k).A_t + Q_t \quad (2)$$

Update:

$$K_t(k+1) = \frac{P_t(k+1|k).C_t}{C_t.P_t(k+1|k).C_t + R_t} \quad (3)$$

$$\varepsilon(k+1) = y_t(k+1) - C_t\,.\hat{x}(k+1|k) \quad (4)$$

$$\hat{x}(k+1|k+1) = \hat{x}(k+1|k) + K_t(k+1).\varepsilon(k+1) \quad (5)$$

$$P_t(k+1|k+1) = (I - K_t(k+1).C_t).P_t(k+1|k) \quad (6)$$

Where $\hat{x}(k|k)$ Is the State Estimate at Time (k) Based On the Information at time (k) (Prior State estimate). $\hat{x}(k+1|k)$ Is the Predicted State Estimate at Time $(k+1)$ Based on The Information at time (k). $P_t(k|k)$ is the State Covariance at Time (k) Based On The Information At Time (k) (Prior Error covariance matrix). $P_t(k+1|k)$ Is the Predicted State Covariance at Time $(k+1)$ Based on The Information at Time (k). $\varepsilon(k+1)$ Is the Residual or The Difference Between the Actual Measurement Result at Time $(k+1)$ And the Measurement Estimate Based on The State Prediction (Measurement Residual). $\hat{x}(k+1|k+1)$ Is the State Estimate at Time $(k+1)$ That Has Been Updated (Posterior State Estimate at Time $k+1$). $P_t(k+1|k+1)$ Is the State Covariance at Time $(k+1)$ That Has Been Updated (Posterior Error Covariance Matrix at Time $(k+1)$. A_t Is The State Transition Matrix. C_t Is The Measurement Matrix. Q_t Is The Process Noise Covariance Matrix. R_t Is The Measurement Noise Covariance Matrix. $K(k+1)$ Is the Kalman Gain Matrix at Time $(k+1)$. I Is the Identity Matrix. In Equation (6) the prediction step, we predict the system state at time $k+1$ based on previous information at time k. The state estimate x_t is updated using the state transition matrix A_t, which represents how the state changes from time k to $k+1$. Furthermore, the state covariance P_t is also updated, taking into account the previous state covariance and the process noise Q_t tepresents the uncertainty in the state prediction.

In the update step, we update the state estimate x_t based on the actual measurement at time $k+1$. The Kalman Gain matrix K_t is used to determine how much we will trust the latest measurement and how much we will trust the previous prediction. The residual ε s the difference between the actual measurement and the measurement estimate based on the state prediction. Furthermore, the state estimate and state covariance are updated based on the latest measurement information and the Kalman Gain matrix. These equations collectively represent the KF process and are utilized to achieve accurate and reliable state estimation in dynamic systems while reducing the impact of noise in the measurements.

Within the above equations, the variable state pertains to the specific attribute or parameter being estimated within the dynamic system. For instance, in this paper, this variable state could correspond to factors like light intensity or position. Notably, it is involved in Equations (1), (4), and (5), where the state estimate is calculated, refined, and employed for measurement prediction, respectively. Through adeptly integrating measured data and predictions, the KF process amplifies the accuracy and dependability of state estimation, particularly when confronted with noise in dynamic systems.

G. VHDL Programming

In the course of this research, the VHDL language played a pivotal role in both the XADC and Arty MicroBlaze projects in Fig 2 and Fig 3. This decision was guided by the flexibility and capabilities that VHDL brings to the table. It's noteworthy that when it comes to choosing between Verilog and VHDL, the Vivado platform provides users with the latitude to decide based on their specific requirements and personal preferences. This level of choice, as illustrated in the accompanying image, underscores Vivado's commitment to accommodating diverse needs within the realm of hardware description languages. As the research delved into harnessing the power of VHDL for the XADC and Arty MicroBlaze projects, it exemplified how the Vivado platform empowers users to align their language selection with their project objectives and inclinations.

```
--Copyright 1986-2019 Xilinx, Inc. All Rights Reserved.
----------------------------------------------------------------------------------
--Tool Version: Vivado v.2019.1 (win64) Build 2552052 Fri May 24 14:49:42 MDT 20
--Date        : Fri Jun  9 14:45:29 2023
--Host        : LAPTOP-04PTB4FM running 64-bit major release  (build 9200)
--Command     : generate_target design_1_wrapper.bd
--Design      : design_1_wrapper
--Purpose     : IP block netlist
----------------------------------------------------------------------------------
library IEEE;
use IEEE.STD_LOGIC_1164.ALL;
library UNISIM;
use UNISIM.VCOMPONENTS.ALL;
entity design_1_wrapper is
  port (
    Vaux12_v_n : in STD_LOGIC;
    Vaux12_v_p : in STD_LOGIC;
    Vaux13_v_n : in STD_LOGIC;
    Vaux13_v_p : in STD_LOGIC;
    Vaux14_v_n : in STD_LOGIC;
    Vaux14_v_p : in STD_LOGIC;
    Vp_Vn_v_n : in STD_LOGIC;
    Vp_Vn_v_p : in STD_LOGIC
  );
end design_1_wrapper;
```

Fig 2. VHDL for XADC on Vivado

```
--Copyright 1986-2019 Xilinx, Inc. All Rights Reserved.
----------------------------------------------------------------------------------
--Tool Version: Vivado v.2019.1 (win64) Build 2552052 Fri May 24 14:49:42 MDT 2019
--Date        : Fri Jun  2 14:20:29 2023
--Host        : LAPTOP-04PTB4FM running 64-bit major release  (build 9200)
--Command     : generate_target design_1_wrapper.bd
--Design      : design_1_wrapper
--Purpose     : IP block netlist
----------------------------------------------------------------------------------
library IEEE;
use IEEE.STD_LOGIC_1164.ALL;
library UNISIM;
use UNISIM.VCOMPONENTS.ALL;
entity design_1_wrapper is
  port (
    ddr3_sdram_addr : out STD_LOGIC_VECTOR ( 13 downto 0 );
    ddr3_sdram_ba : out STD_LOGIC_VECTOR ( 2 downto 0 );
    ddr3_sdram_cas_n : out STD_LOGIC;
    ddr3_sdram_ck_n : out STD_LOGIC_VECTOR ( 0 to 0 );
    ddr3_sdram_ck_p : out STD_LOGIC_VECTOR ( 0 to 0 );
    ddr3_sdram_cke : out STD_LOGIC_VECTOR ( 0 to 0 );
    ddr3_sdram_cs_n : out STD_LOGIC_VECTOR ( 0 to 0 );
    ddr3_sdram_dm : out STD_LOGIC_VECTOR ( 1 downto 0 );
    ddr3_sdram_dq : inout STD_LOGIC_VECTOR ( 15 downto 0 );
    ddr3_sdram_dqs_n : inout STD_LOGIC_VECTOR ( 1 downto 0 );
    ddr3_sdram_dqs_p : inout STD_LOGIC_VECTOR ( 1 downto 0 );
```

Fig 3. VHDL for Arty MicroBlaze on Vivado

In the actual Vivado software utilization, VHDL takes on a pivotal role, serving as the programming language of choice for both the configuration of the XADC module and the creation of the Arty MicroBlaze project. VHDL presents itself as a structured and robust medium for intricately delineating the behaviours and functionalities of hardware components. This capability extends to configuring the XADC module, where VHDL enables engineers to define its operations meticulously. This empowers the module to adeptly process analogue signals, converting them into digital data with precision. This strategic application of VHDL allows for customization and aligns the XADC's behaviour seamlessly with the project's specific demands.

Similarly, VHDL proves its mettle in the context of the Arty MicroBlaze project. This soft-core processor, a linchpin in embedded system development, finds its architectural essence defined through VHDL. Engineers harness its prowess to sculpt the MicroBlaze's fundamental attributes-its instruction set, memory interfaces, and more. This ensures that the processor is not just a component but an intricately tailored entity that harmonizes optimally with the project's needs. The deployment of VHDL here underscores its versatility in addressing complex, customized hardware description tasks.

3. RESULT AND DISCUSSIONS

This chapter discusses the Design of LEDs for data transmission, the Design of the Receiver using the FPGA Arty Xilinx and Photodetectors hardware, and the utilization of Vivado software to observe the transmission of light signal data sent by the Photodetectors. Additionally, this chapter will also present the results of the LEDs and Photodetectors system implemented with Xilinx FPGA Arty A7-35T on Vivado. The outcomes of implementing the KF on the Vivado Design Suite using the Xilinx SDK will also be discussed. This research will reveal the Performance of KF Using the values of RMSE or for each KF result. Furthermore, the analysis of the results will encompass the power utilization and implementation generated by the KF in the Vivado Design Suite, and it will compare the utilization and implementation of power between the KF 1D project and the KF 2D. All results and analyses are presented comprehensively to provide a clear understanding of the efficiency and effectiveness of the entire developed system.

A. Hardware Configuration

In this section, we systematically designed an LED system to facilitate data transmission through light signals generated by LEDs. A crucial step was taken to connect the Photodetectors sensor to the Xilinx FPGA Arty A7-35T hardware, utilizing the VHDL language within the Vivado Design Suite software. This step is crucial because if not connected properly, the sensor will not function effectively. After completing the VHDL

programming in Vivado, the next crucial step is to implement the design from Vivado Software to the Xilinx FPGA Arty A7 hardware. However, before proceeding with the implementation, three key stages must be completed in the Vivado Software: Run Synthesis, Run Implementation, and Generate bitstream. The illustration of the connection between the Photodetectors sensor and Xilinx FPGA Arty A7 through the Analog Output Port on the sensor and the ADC Connectors on the FPGA is shown in Fig 5 above. If all three stages are successfully completed, the designed programming can be directly implemented into the Xilinx FPGA Arty A7 hardware, enabling the Photodetectors sensor, which is already connected to the Xilinx FPGA Arty A7, to operate optimally in reading the data transmitted by the light.

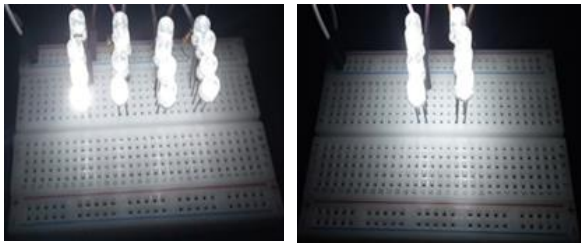

Fig 4. LED source of 4 and 8 for testing

In this research, a systematic design of LED systems has been conducted to facilitate data transmission through light signals generated by the LEDs. The primary objective of this design is to achieve optimal effectiveness and efficiency in the process of data transmission through light signals. To realize this objective, configurations employing 16 and 8 units of 5mm LEDs have been utilized and organized in a 4x4 and 4x2 arrangement, respectively, as illustrated in Fig 4. Through this strategic arrangement of LEDs, it is anticipated that the transmission of data via light signals can be executed in an optimized and efficient manner.

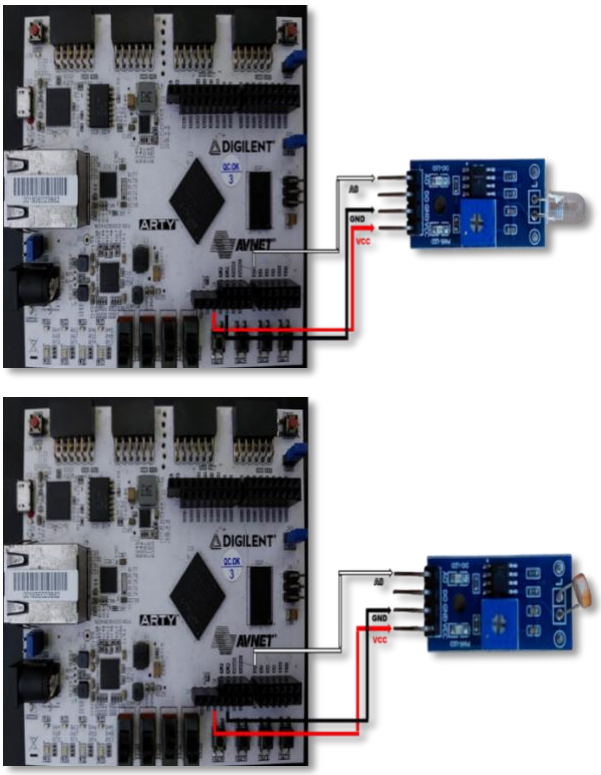

Fig 5. Connecting FPGA Arty 7 to Photodiode & Photoresistor

Important steps must be taken to connect the Photodetectors sensor to the Xilinx FPGA Arty A7-35T hardware, which is done by connecting it through VHDL language in the Vivado Design Suite software. This connecting process is crucial because if not properly connected, the sensor will not function properly. After completing the programming using VHDL in Vivado, the next step is to carry out the implementation from the Vivado Software to the Xilinx FPGA Arty A7 hardware. However, before performing the implementation, there are three stages that must be done in the Vivado Software, namely Run Synthesis, Run Implementation, and Generate bitstream. The illustration of the connection between the Photodetectors sensor and Xilinx FPGA Arty A7 through the Analog Output Port on the sensor and the ADC Connectors on the FPGA can be seen in Fig 5 above. If all three stages have been successfully completed, the designed programming can be directly implemented into the Xilinx FPGA Arty A7 hardware, enabling the Photodetectors sensor, which is already connected to the Xilinx FPGA Arty A7, to work optimally in reading the data sent by the light.

B. Photodetectors Testing

This section shows the result and analysis involving comprehensive testing of measurement results from PD LM393 and PR LM393, utilizing variations of 16 LEDs and 8 LEDs.

Table 1. Measurement of PD

PD LM393	**16 Leds**		**8 Leds**	
Distance (cm)	*Lux meter (lx)*	*PD measure (v)*	*Lux meter (lx)*	*PD measure (v)*
10	2183,8	0,0642	2026,4	0,1957
20	1996,6	0,0363	797,5	0,215
30	893,5	0,0187	360,1	0,4125
40	416,7	0,0225	221,8	0,4433
50	373,5	0,0461	175,6	0,5378
60	231,7	0,0825	96,5	0,4798
70	150,9	0,2631	79,3	0,5071
80	139,8	0,2411	59,3	0,6475
90	101,2	0,4638	41,3	0,8178
100	66	0,7828	42	0,9791

Table 1 contains measurement data employing PD LM393 with variations of 16 LEDs and 8 LEDs. The data encompasses the distance between PD LM393 and LEDs, light intensity gauged by a Lux Meter (lx), and output voltage measured via Vivado software.

Fig 6 Shows data through a graph, showcasing output voltage measurements from PD LM393 at varying distances using 16 LEDs (blue line) and 8 LEDs (orange line). The recorded data includes distance (cm), light intensity (lux) measured by a Lux Meter, and output voltage (V) gauged via the Vivado device. The graph reflects the direct relationship between increased distance and augmented output voltage for both LED variations. The 16 LEDs variation exhibits output voltage ranging from 0.0642 V to 0.7828 V, while the 8 LEDs variation spans from 0.1957 V to 0.9791 V.

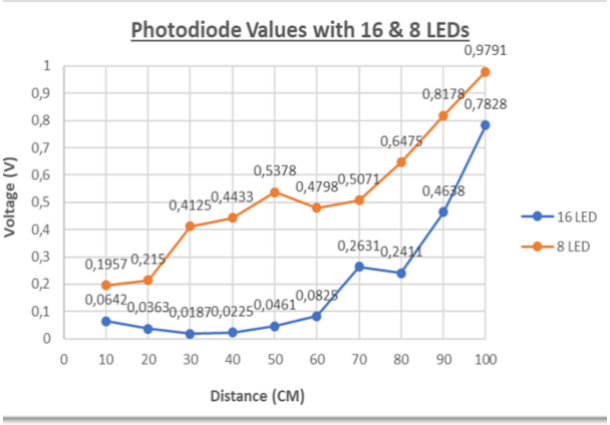

Fig 6. Voltage output on PD LM393

Comparing measurements between 16 LEDs and 8 LEDs with PD LM393 uncovers intriguing insights. At equal distances, the employment of 8 LEDs yields higher output voltage than 16 LEDs. Other factors, including PD LM393 characteristics and Implementation of the Process, can influence output voltage and light intensity in measurements. However, the data suggests that 8 LEDs offer enhanced responsiveness, generating higher output voltage in PD LM393 when contrasted with 16 LEDs.

Table 2. Measurement of PR LM393

PR LM	**16 Leds**		**8 Leds**	
Distance (cm)	*Lux meter (lx)*	*PR measure (V)*	*Lux meter (lx)*	*PR measure (V)*
10	4709,9	0,064	1179,4	0,1818
20	2273,1	0,1651	992,6	0,3587
30	994,4	0,2978	478,4	0,5339
40	492,6	0,3809	203,4	0,7532
50	335,5	0,6151	175	0,8668
60	203,5	0,6675	113,8	0,9757
70	113,1	0,7828	68,1	0,9287
80	112,4	0,8571	51,4	0,9425
90	105	0,8767	36,4	0,9459
100	80,3	0,8834	26,4	0,9485

Table 2 displays measurement data using PR LM393 with variations of 16 LEDs and 8 LEDs. The data encompasses distance between PR LM393 and LEDs, light intensity measured in lux via a Lux Meter, and output voltage measured in volts using Vivado Software. The results yield significant insights. Firstly, measured light intensity diminishes as the distance between PR LM393 and LEDs increases, evident from decreasing Lux Meter values at each distance. Particularly noteworthy is the substantial intensity drop between 10 cm

and 100 cm distances. Secondly, the output voltage, measured through Vivado Software, follows a similar pattern, increasing as the distance between PR LM393 and LEDs grows. This trend applies to measurements using both 16 LEDs and 8 LEDs. A comparison between 16 LEDs and 8 LEDs with PR LM393 reveals higher light intensity and smaller output voltage for 16 LEDs at equal distances.

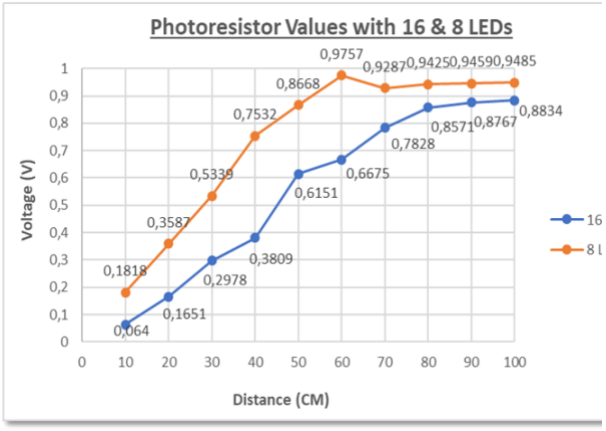

Fig 7. Voltage output on PR LM393

Based on Fig 7, it is evident that the output voltage from PR LM393 shows a proportional increase with an increase in the distance between PR LM393 and LEDs, both in variations of 16 LEDs and 8 LEDs. The range of output voltage for the 16 LEDs variation ranges from 0.064 V to 0.8834 V, while for the 8 LEDs variation, the range of output voltage is 0.1818 V to 0.9485 V. In the context of comparing the measurement results using 16 LEDs and 8 LEDs with PR LM393, some interesting findings are discovered. At the same distance, the use of 8 LEDs results in a relatively higher output voltage compared to the use of 16 LEDs. This indicates that the use of 8 LEDs can generate a stronger signal in the PR LM393. based on the overall results and the data presented, that the use of 8 LEDs provides relatively better responsiveness in generating higher output voltage in PR LM393 compared to the use of 16 LEDs.

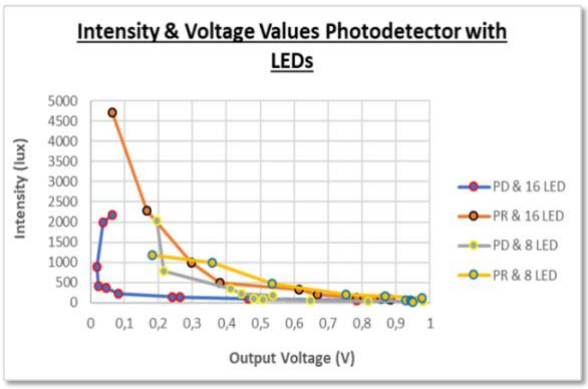

Fig 8. Mapping of measured light intensity on PD output voltage

Fig 8 illustrates output voltage measurements of Photodetectors concerning received light intensity. Data encompasses PD LM393 and PR LM393 sensors using 8 and 16 LEDs. The output voltage is in volts, light intensity is in lux. Four lines represent each kind of PD LM393 and PR LM393 with 8 and 16 LEDs. Blue and orange lines show PD LM393 and PR LM393 values using 16 LEDs. Grey and yellow lines show PD LM393 and PR LM393 values using 8 LEDs. In 16 LEDs, PD LM393 output voltage (blue line) tends to be lower than PR LM393 (orange line) for each distance and light intensity, indicating PR LM393's higher response to light. With 8 LEDs, the yellow line (PR LM393) still surpasses the grey line (PD LM393) in response, but the difference is smaller than with 16 LEDs. Comparative results reveal PR LM393's higher sensitivity to light intensity detection. LED use influences the response of both components, with 8 LEDs yielding a higher output voltage response due to lower light intensity. In conclusion, the graph compares PD LM393 and PR LM393 in light intensity measurement using 8 and 16 LEDs. PR LM393 is more sensitive and using 8 LEDs generates more responsive measurements, indicating PR LM393's superior sensitivity and 8 LEDs' effectiveness in capturing light changes.

C. Kalman Filter Implementations

This section, based on these results an in-depth analysis was carried out through various tables and figures to compare the measurement values with the KF estimation algorithm for the PD LM393 and PR LM393 sensors using different LED configurations. Table III provides a comparative overview of KF measurements and values, highlighting the

improvement in KF accuracy in both LED scenarios. The corresponding Figure 9 graphically represents these values, demonstrating the effectiveness of the KF algorithm in increasing accuracy for both types of LEDs.

Table 3. KF Performance with PD LM393

	16 Leds		8 Leds	
Distance (cm)	***PD meas(v)***	***KF (v)***	***PD meas (v)***	***KF (v)***
10	0,0642	0,0661	0,1957	0,1958
20	0,0363	0,0361	0,215	0,2149
30	0,0187	0,0187	0,4125	0,4124
40	0,0225	0,0225	0,4433	0,4433
50	0,0461	0,0460	0,5378	0,5374
60	0,0825	0,0826	0,4798	0,4713
70	0,2631	0,2634	0,5071	0,5030
80	0,2411	0,2412	0,6475	0,6527
90	0,4638	0,4672	0,8178	0,8196
100	0,7828	0,7835	0,9791	0,9799

Table 3 compares measurement and KF values for PD LM393 using 8 LEDs and 16 LEDs. Differences exist between Measurement (v) and KF (v) values at each distance, favoring KF's accuracy enhancement in both LED scenarios. Overall, 16 LEDs yield more accurate results than 8 LEDs, evidenced by smaller Measurement-KF differences. Data highlights KF's effectiveness in enhancing PD LM393 measurement accuracy, particularly with 16 LEDs, offering improved outcomes compared to 8 LEDs.

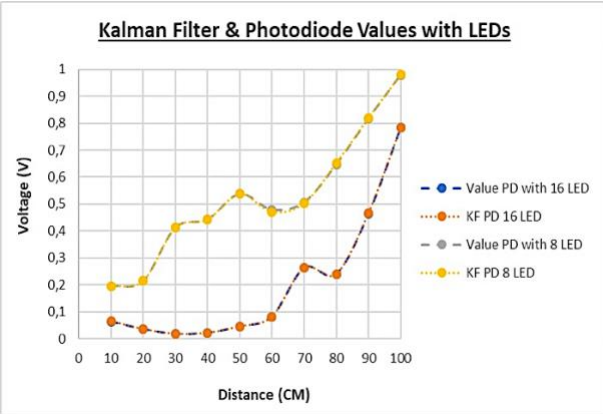

Fig 9. KF Performance with PD LM393

Fig 9 shows a line graph showcasing four variables. The blue line signifies Original Values from PD LM393 measurements with 16 LEDs, while the orange line represents KF algorithm output using 16 LEDs. Also, a gray line shows Original Values from PD LM393 measurements with 8 LEDs, and the yellow line represents KF algorithm output using 8 LEDs. Data on the graph highlights significant differences between measurements using 16 LEDs and 8 LEDs for PD LM393. At 10 cm distance, Sensor Measurement (V) is 0.0642V for 16 LEDs, contrasting with 0.1957V for 8 LEDs. This trend continues at other distances, with 16 LEDs yielding lower Sensor Measurements (V) compared to 8 LEDs. However, KF implementation for both types of measurements demonstrates KF (V) values approximating original Sensor Measurements (V). This implies KF's effectiveness in improving measurement accuracy for both LED types, aligning them closer to PD LM393 measurements.

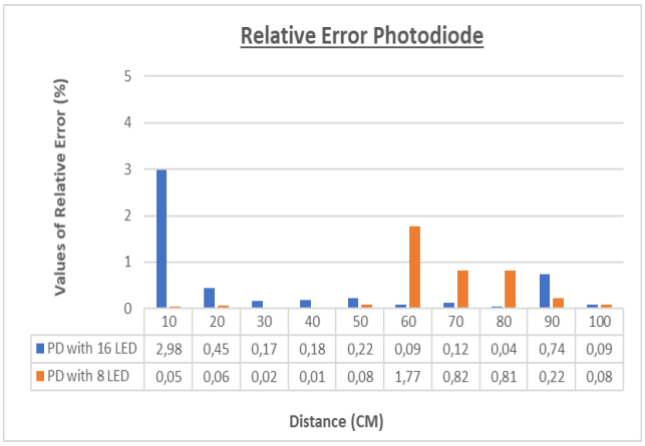

Fig 10. Relative errror of KF with PD

Fig 10 illustrates a comparison of the data results, indicating that measurements using PD LM393 with 8 LEDs yield lower relative errors compared to the use of 16 LEDs at various distances. However, at greater distances (60 - 80 CM), the relative error values with 8 LEDs are comparatively higher. Conversely, for measurements taken at other distances, the configuration with 8 LEDs demonstrates better stability and lower relative error values. In terms of providing higher accuracy in estimating received light intensity, it can be concluded that the configuration with 8 LEDs delivers more precise results across different distances.

Table 4 compares the measurement results and KF estimation values for PR LM393 using 16 LEDs and 8 LEDs. The table includes "Measurement (V)" and "KF (V)" columns for both LED configurations. The KF algorithm effectively approximates Measurement (V) values in both cases, aligning KF (V) values

with the original measurements. Despite significant differences between measurements using 16 LEDs and 8 LEDs with PR LM393, the KF algorithm mitigates these differences, aligning both LEDs types' results with PR LM393's true values.

Table 4. KF Performance with PR LM393

	16 Leds		8 Leds	
Distance (cm)	*PR measure (v)*	*KF (v)*	*PR measure (v)*	*KF (v)*
10	0,064	0,06415	0,1818	0,1812
20	0,1651	0,16499	0,3587	0,35884
30	0,2978	0,29791	0,5339	0,53349
40	0,3809	0,38091	0,7532	0,75374
50	0,6151	0,61518	0,8668	0,86804
60	0,6675	0,66989	0,9757	0,97552
70	0,7828	0,78463	0,9287	0,92876
80	0,8571	0,85814	0,9425	0,94257
90	0,8767	0,87671	0,9459	0,94584
100	0,8834	0,88438	0,9485	0,94855

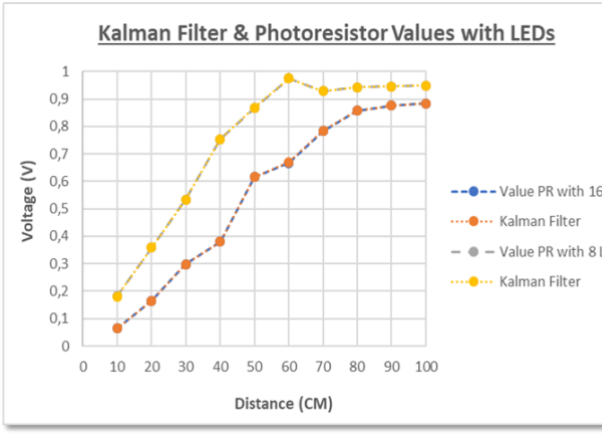

Fig 11. KF Performance with PR LM393

Fig 11 shows a graph displaying four variables, representing PR LM393 measurements using 16 LEDs and 8 LEDs. The blue line illustrates True Values from measurements with PR LM393 and 16 LEDs, while the orange line depicts the KF algorithm output at each position using the same setup. Additionally, the grey line signifies True Values from measurements using PR LM393 and 8 LEDs, with the yellow line showcasing KF algorithm results for the corresponding positions with 8 LEDs. Differences exist between readings obtained by PR LM393 using 16 LEDs and 8 LEDs. At a 10 cm distance, Measurement (V) is 0.064 V for 16 LEDs and 0.1818 V for 8 LEDs. This trend continues at other distances, indicating lower Measurement (V) values with 16 LEDs than with 8 LEDs. Nevertheless, implementing the KF algorithm for both scenarios leads to KF (V) values approximating or matching True Values. This underscores the KF algorithm's effectiveness in enhancing measurement outcomes for both LEDs types, aligning them with PR LM393's true values.

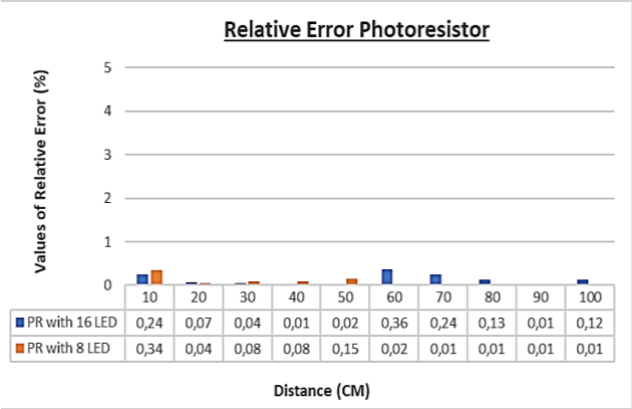

Fig 12. Relative error of KF with PR LM393

Fig 12 illustrates a comparison of the outcomes from utilizing 16 & 8 LEDs within the PR LM393 configuration. This comparison showcases a more consistent and accurate estimation of the received light intensity across various distances when employing 8 LEDs. Although there is a slightly elevated Relative Error Value observed with the 8 LEDs at specific points (10, 30, 40, and 50 CM), the overall trend highlights the superiority of the 8 LED configuration in mitigating relative errors. Consequently, these findings conclusively underscore the enhanced capability of the PR LM393 configuration with 8 LEDs in providing precise and consistent estimations of light intensity across varying distances.

Table 5 compares measured values and KF algorithm estimations for photodiode (x) and photoresistor (y) sensors with 16 LEDs. KF estimations closely match actual measurements, indicating accurate estimations. The small difference between them underscores estimation accuracy. Notably, the gap narrows as distance increases, highlighting KF's superiority in accurate estimations at greater distances. Overall, 2D KF use for both sensors effectively reduces fluctuations and enhances measurement estimation precision.

Table 5. Performance of KF 2D with 16 LED

	Photodiode (x)	**Photoresistor (y)**

Dist(cm)	*PD (v)*	*KFx(v)*	*PR (v)*	*KFy(v)*
10	0,108	0,0972	0,0678	0,0610
20	0,0424	0,0382	0,1624	0,1462
30	0,0182	0,0164	0,3002	0,2702
40	0,023	0,0207	0,3802	0,3429
50	0,044	0,0396	0,6188	0,5569
60	0,0846	0,0761	0,6998	0,6298
70	0,2854	0,2569	0,8072	0,7265
80	0,244	0,2196	0,8598	0,7738
90	0,480	0,4320	0,8772	0,7895
100	0,8172	0,7355	0,8884	0,7996

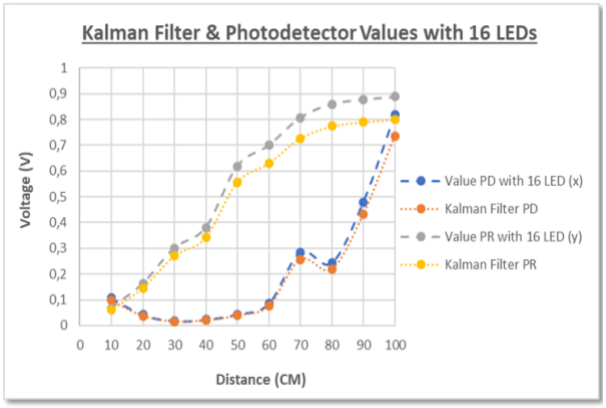

Fig 13. Performance of KF 2D with 16 LED

Fig 13 depicts a comparison between measurement results and 2D KF estimations for PD LM393 and PR LM393 sensors with 16 LEDs. The 2D KF implementation effectively reduces fluctuations and enhances estimation stability. In PD LM393, fluctuations in measurement values diminish with KF estimations approximating actual values, especially at greater distances. Similarly, PR LM393 experiences reduced fluctuations and improved estimations with KF implementation, showcasing accuracy enhancement. Overall, 2D KF implementation significantly reduces fluctuations and provides accurate estimations for both sensors with 16 LEDs.

Based on Table 6, it can be seen that the use of the 2D KF on the PD LM393 sensor (x) and PR LM393 sensor (y) with 8 LEDs yielded good results. The comparison between the measurement values and the estimated data showed small differences, indicating high estimation accuracy. At greater distances, the differences between the measurements and estimations decreased, indicating an improvement in estimation accuracy. Overall, the 2D KF was relatively effective in reducing fluctuations and enhancing measurement accuracy on the Photodetectors sensor with 8 LEDs.

Table 6. Performance of KF 2D with 8 LED

	Photodiode (x)		**Photoresistor (y)**	
Dist(cm)	***PD (v)***	***KFx(v)***	***PR (v)***	***KFy(v)***
10	0,1956	0,17604	0,168	0,1512
20	0,2124	0,19116	0,371	0,3339
30	0,411	0,3699	0,5206	0,46854
40	0,4446	0,40014	0,771	0,6939
50	0,5896	0,53064	0,9008	0,81072
60	0,366	0,3294	0,9704	0,87336
70	0,4984	0,44856	0,9284	0,84556
80	0,752	0,6768	0,9446	0,85014
90	0,8416	0,75744	0,9442	0,84978
100	0,9864	0,88776	0,9488	0,85392

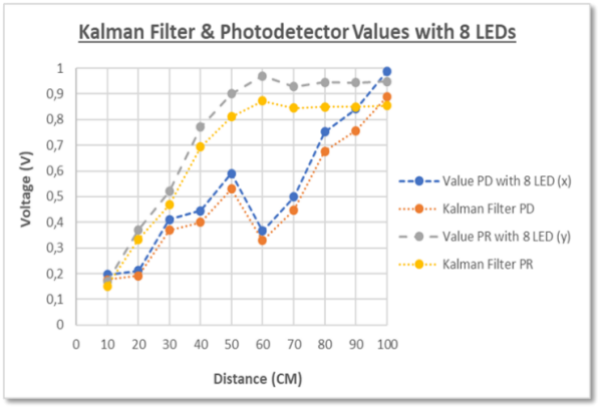

Fig 14. Performance of KF 2D with 16 LED

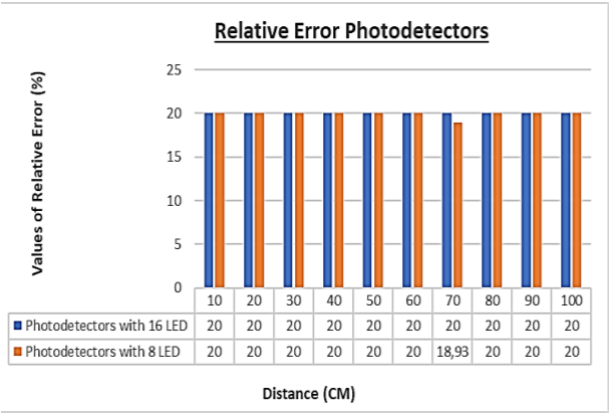

Fig 15. Relative error of KF 2D

Fig 14 shows a comparison between measurements and 2D KF estimations on PD LM393 and PR LM393 sensors with 8 LEDs. Fluctuations in PD LM393 measurements decrease with KF implementation, leading to more stable estimations near true values. A similar trend was observed in PR LM393 measurements, where KF reduces fluctuations at greater distances, enhancing stability. Differences between measurements and KF estimations decrease at longer distances, signifying accuracy improvement.

Fig 15 illustrates a comparative analysis of the utilization of Photodetectors LM393 with 16

& 8 LED configurations, showcasing a consistent 20% relative error value at each measurement point spanning distances from 10 to 100 CM for both configurations. Notably, when employing the 8 LED configuration at a distance of 70 CM, a marginal reduction in the relative error value to 18.93% is observed, while the 16 LED configuration remains constant at 20%. Overall, it is evident that both configurations exhibit similar relative error performance across various measurement distances. These findings imply that both the 16 LED and 8 LED configurations yield consistent relative error values at specific distances. The outcomes underscore a comparable and stable relative error performance for the Photodetectors LM393 configurations employing 16 & 8 LEDs across varying distances.

D. Root mean square error

RMSE is a widely used evaluation metric in regression analysis and forecasting, assessing the accuracy of prediction models by measuring the squared differences between predicted and actual values, followed by computing the square root of the average of these squared differences [16].

This section examines the outcomes of applying the KF method to PD LM393 and PR LM393 sensors with varying LED setups. The goal is to assess the performance and prediction error levels of each approach in measuring LED-emitted light. Four RMSE results are obtained, representing prediction error for KF on PD LM393 with 16 LEDs, PD LM393 with 8 LEDs, PR LM393 with 16 LEDs, and PR LM393 with 8 LEDs. RMSE serves as a comparative indicator for prediction accuracy across methods. Additionally, RMSE values are calculated for 2D KF on PD LM393 with 16 LEDs (x) and PR LM393 with 16 LEDs (y), as well as PD LM393 with 8 LEDs (x) and PR LM393 with 8 LEDs (y). This analysis unveils accuracy and effectiveness differences among methods, highlighting factors affecting prediction outcomes. The RMSE calculation formula is as follows:

$$RMSE = \sqrt{\frac{1}{n}\sum_{i=1}^{n}(f_i - o_i)^2} \qquad (7)$$

Where Σ is the summation o all values. f is the predicted value. os Measurements Value. $(f_i - o_i)^2$ are the differences between predicted and observed values and Squared. n is the total sample size [16]. The RMSE values obtained in Table 7 and Table 8 are used as specific evaluation metrics for measurement results within the range of 0.1 to 1.

Table 7. RMSE Values of KF 1D

	E (v)	RMSE
PD, 16 LED	0,022642	2,2642
PR, 16 LED	0,016914	1,6914
PD, 8 LED	0,053404	5,3404
PR, 8 LED	0,017076	1,7076

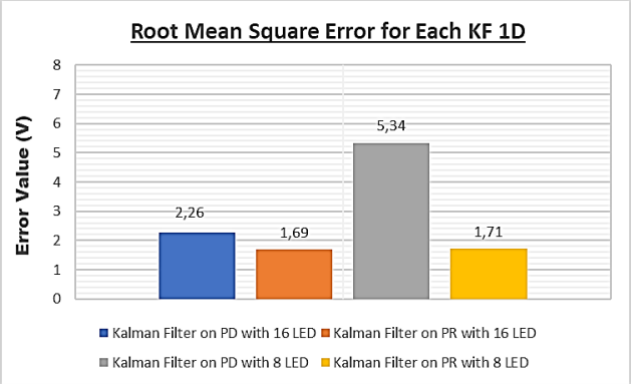

Fig 16. RMSE of KF 1D

In the Graph in Fig 16, four variables are represented by different colours. The KF values for PD LM393 with 16 LEDs are shown in blue, while the KF values for PR LM393 with 16 LEDs are displayed in orange. Furthermore, the KF values for PD LM393 with 8 LEDs are depicted in grey, and the KF values for PR LM393 with 8 LEDs are presented in yellow. From the above RMSE values, we can observe the performance comparison of the KF on two types of systems, namely the PD LM393 system and the PR LM393 system, both using either 16 or 8 LEDs. First, on the system with 16 LEDs, The RMSE results show that the KF in combination with PD LM393 has an RMSE of approximately $(2{,}26\ x\ 10^{-2}\ V)$, while with PR LM393 has an RMSE of approximately $(1{,}69\ x\ 10^{-2}\ V)$. Next, for the system with 8 LEDs, the RMSE results show that KF & PD LM393 has an RMSE of approximately $(5{,}34\ x\ 10^{-2}\ V)$, while KF & PR LM393 has an RMSE of approximately $(1{,}71\ x\ 10^{-2}$). Overall, the results show that KF in combination with the PR LM393 system tends to provide relatively more accurate estimations

and can be more effective in reducing noise and fluctuations in measurements. compared to the PD LM393 system in both cases, with 16 or 8 LEDs. Although the difference in RMSE is relatively small, the results suggest a preference for using KF with the PR LM393 system in VL application.

Table 8. RMSE Values of KF 2D

	E (V)	RMSE
16 LED	0,78478	7,8478
8 LED	1,2778	12,778

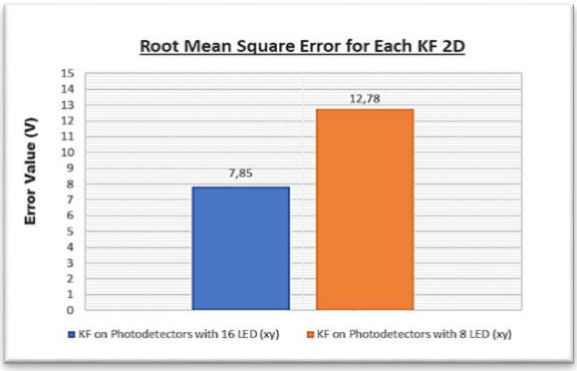

Fig 17. RMSE of 2D KF

Based graph in Fig 17, two variables are represented by different colours. The KF values for Photodetectors with 16 LEDs (xy) are displayed in blue, while the KF values for Photodetectors with 8 LEDs (xy) are shown in orange. From the above RMSE values, we can observe the performance of the KF in two types of systems, namely the Photodetectors LM393 system with 16 LEDs and 8 LEDs. First, let's review the results for the Photodetectors LM393 system with 16 LEDs. The RMSE result for KF in this system is approximately $7{,}8478\ x\ 10^{-1}\ V$. Next, in the Photodetectors LM393 system with 8 LEDs, the RMSE result for KF is approximately $12{,}778\ x\ 10^{-1}\ V$. `Similar to the previous system, the estimations provided by KF have small errors compared to the true measurement values. From these results, it can be concluded that in both cases, with 16 LEDs and 8 LEDs, KF is relatively successful in providing accurate and stable estimations. The lower RMSE values indicate good accuracy between the KF estimation results and the true measurement values. This demonstrates the effectiveness of KF in reducing noise and improving estimation accuracy in the Photodetectors LM393 system with 16 or 8 LEDs.

E. Utilization of FPGA Resources

The stage in the analysis using the Vivado Design Suite software is to perform a synthesis, where the results of this process will provide results in the form of information on the percentage of resources resulting from the utilization of the Xilinx FPGA Arty A7-35T board for the project being carried out.

Table 9. Utilization of FPGA Arty A7-35T

Project	Resources	Utilization (unit)	Available (unit)	Utilization (%)
KF 1D	LUT	1.152	20.800	5.54
	FF	65	41.600	0.16
	DSP	2	90	2.22
	I/O	51	210	24.29
KF 2D	LUT	2.320	20.800	11.15
	FF	193	41.600	0.46
	DSP	4	90	4.44
	I/O	98	210	46.47

Table 9 represents the post-synthesis comparison results for the KF 1D & 2D project, analyzed using vivado Software with Xilinx FPGA Arty A7-35T hardware. This table provides information about the FPGA resource utilization, such as Look Up Table (LUT), Flip Flop (FF), DSP, and I/O, along with the percentage of utilization that occurred in the project.

The Graph in Fig 18, for the implementation of 1D KF, the resource utilization is as follows: 1,152 LUT, 65 FF, 2 DSP, and 51 I/O. The percentage of resource utilization on Xilinx FPGA Arty A7-35T for LUT is 5.54%, FF 0.16%, DSP 2.22%, and I/O 24.29%. Meanwhile, for the implementation of 2D KF, the resource utilization on Xilinx FPGA Arty A7-35T is as follows: 2,320 LUT, 193 FF, 4 DSP, and 98 I/O. The percentage of resource utilization on Xilinx FPGA Arty A7-35T for LUT is 11.15%, FF 0.46%, DSP 4.44%, and I/O 46.47%. From the results, several conclusions can be drawn. First, the implementation of 2D KF relatively utilizes more Xilinx FPGA Arty A7-35T resources compared to the implementation of 1D KF. This is evident from the higher numbers in LUT, FF, DSP, and I/O utilization for the 2D KF implementation. Second, the percentage of resource utilization on Xilinx FPGA Arty A7-35T for the 2D KF

implementation is also relatively higher than the 1D KF implementation, indicating a higher level of Xilinx FPGA Arty A7-35T resource utilization in the 2D KF implementation.

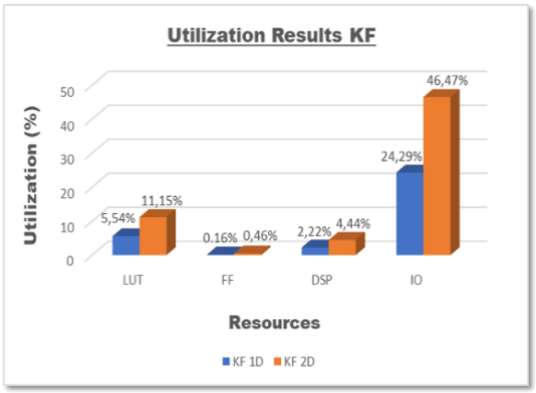

Fig 18. FPGA Resource Utilization of KF 1D & 2D

F. Power Usage

In This Section checking the implementation of power, use the power analysis feature in Vivado to estimate power using post-synthesis. The activity performed by the expended power is determined by the number of I/O Block pins used. The more I/O Block pins, the more power is released. Once the power analysis is complete, the summary will show to review the total on-chip power.

Table 10 shows KF 1D relatively lower power consumption compared to KF 2D in all aspects of power usage, including signals, logic, DSP, and I/O. However, both KF 1D and KF 2D still maintain relatively minimal power consumption in percentage scale of the total available power.

Table 10. Power usage of KF 1D & 2D on Xilinx FPGA Arty A7-35T

	On Chip Power					
Projects	***Dynamic (W)***	***Device Static(W)***	***Signals (W)***	***Logic (W)***	***DSP (W)***	***I/O (W)***
KF 1D	56.033	0.327	16.121	18.961	1.914	19.038
KF 2D	112.954	0.327	33.427	37.736	4.020	37.772

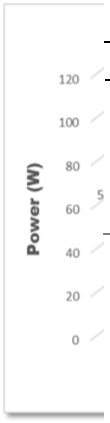

Fig 19. Power usage of KF 1D & KF 2D

The Graph in Fig 19, illustrates significant differences in power consumption between the two projects, KF 1D and KF 2D, across various aspects of power usage. In terms of dynamic power consumption, KF 2D requires relatively twice the amount of power compared to KF 1D. This indicates that KF 2D has a higher level of complexity and power requirements compared to KF 1D. The KF 1D project consumes 56.033 W (99%) in dynamic power, mainly from circuit switching. Device static power is low at 0.327 W (1%). Logic uses the most power at 18.961 W (34%), followed by IO at 19.038 W (34%) and DSP at 1.914 W (3%). KF 2D has double the power of KF 1D, with 112.954 W (99%) in dynamic power and 0.327 W (1%) in device static power. Logic remains the biggest power consumer at 37.736 W (33%), while DSP and IO each use 4.020 W (4%) and 37.772 W (33%), respectively.

4. CONCLUSION

The research demonstrates that Using 8 LEDs in both PD LM393 and PR LM393 configurations yields lower relative errors compared to 16 LEDs across distances, with better stability and accuracy at shorter distances. Photodetectors LM393 with 16 & 8 LEDs show consistent 20% relative errors from 10 to 100 CM, and the 8 LED setup slightly reduces to 18.93% at 70 CM, while the 16 LED remains at 20%. KF implementation with PR LM393 yields superior outcomes, evident from the lower RMSE values of approximately $(1{,}69\ x\ 10^{-2}\ V\ )$ for 16 LEDs and $(1{,}71\ x\ 10^{-2})$ for 8 LEDs. The 2D KF achieves an RMSE of about $(7{,}8478\ x\ 10^{-1}\ V\ )$, showcasing effective noise reduction and measurement fluctuation management in the LM393 Photodetectors system with 16 LEDs. The research successfully implements Xilinx FPGA Arty A7-35T to process data from PD LM393 and PR LM393 sensors for light measurement and further processing. Utilizing the KF algorithm on Xilinx FPGA Arty A7-35T leads to relatively accurate estimations, reduced noise, and improved measurement accuracy. The comparison of resource utilization between KF 1D and KF 2D on Xilinx FPGA Arty A7-35T highlights relatively the higher complexity

of KF 2D. The power consumption comparison underscores that KF 2D requires twice the power of KF 1D, indicating relatively higher complexity and power needs. Furthermore, testing reveals that the KF implementation, coupled with PD LM393 and PR LM393 sensors and 16 LED/8 LED light sources, consistently provides relatively accurate results. Overall, the research establishes the viability of Xilinx FPGA Arty A7-35T and KF Implementation for light measurement using Photodetectors.

ACKNOWLEDGMENT

The Authors wish to convey their sincere gratitude for the part of the Work in this paper that was funded by MRG UAI 2022. This financial support has played a pivotal role in facilitating and enhancing the research endeavours delineated within this paper. Additionally, the authors extend their heartfelt appreciation to all those who have contributed to this work, including individuals whose contributions may not be enumerated individually.

REFERENCES

[1] M. E. Hisham Abuella, "Hybrid RF/VLC Systems: A Comprehensive Survey on Network Topologies, Performance Analyses, Applications, and Future Directions," *IEEE Access*, vol. vol. 9, no. 0.1109/ACCESS.2021.3129154, p. 160402–160436, 2021.

[2] X. F. Parth H. Pathak, "Visible Light Communication, Networking, and Sensing: A Survey, Potential and Challenges," *IEEE Commun. Surv. Tutorials*, Vols. vol. 17, no. 4, no. doi: 10.1109/COMST.2015.2476474, p. 2047–2077, 2015.

[3] R. L. A. Navin Kumar, "Visible Light Communication Systems Conception and VIDAS," *IETE Technical Review* , vol. 25(6), no. DOI:10.4103/0256-4602.45428, 2008.

[4] A. R. Ndjiongue, "Visible Light Communications (VLC) Technology," *Journal of Electrical and Electronic Engineering Science*, no. DOI:10.1002/047134608X.W8267, 2015.

[5] "Artix 7 FPGA Family," 03 Jul 2023. [Online]. Available: https://www.xilinx.com/products/silicon-devices/fpga/artix-7.html.

[6] "Vivado Design Suite - HLx Editions," 03 Jul 2023. [Online]. Available: https://www.xilinx.com/support/documentation-navigation/development-tools/hardware-development/vivado-design-suite.html.

[7] "Definition of HDL PCMAG," 30 Nov 2022. [Online]. Available: https://www.pcmag.com/encyclopedia/term/hdl.

[8] "How to use a photodiode module Canada Robotix," 30 January 2022. [Online]. Available: https://www.canadarobotix.com/blogs/how-to/photodiode-module-guide.

[9] "Electronic Spices LM393 Photosensitive light dependent resistor LDR sensor module Electronic Components Electronic Hobby Kit," 01 July 2023. [Online]. Available: https://www.flipkart.com/electronic-spices-lm393-photosensitive-light-dependent-resistor-ldr-sensor-module-components-hobby-kit/p/itm460235f630c5e.

[10] "5mm LED technical specifications and power characteristics," 03 January 2023. [Online]. Available: https://www.make-it.ca/5mm-led-specifications/.

[11] "FreeRTOS BSP for Xilinx Software Development Kit (SDK)," 26 Juny 2023. [Online]. Available: https://www.freertos.org/RTOS-Xilinx-SDK-BSP.html.

[12] Hisham Abuella, "Hybrid RF/VLC Systems: A Comprehensive Survey on Network Topologies, Performance Analyses, Applications, and Future Directions," *IEEE Access* , no. DOI:10.1109/ACCESS.2021.3129154, p. PP(99), 2021.